

NONLINEAR DYNAMIC MODEL OF A TURBINE BLADE CONSIDERING VIBRATION AND CRACK COUPLING

YUJIANG WANG, DEYI LUO, YUANXING HUANG, YUE PENG, XUDONG WANG,
XINGWANG YAN

*School of Mechanical and Automotive Engineering, Guangxi University of Science and Technology, Liuzhou, China
corresponding author Yuanxing Huang, e-mail: 260013935@qq.com*

HONGMING XIAO, ZHONGLING HUANG

Wuling New Energy Automobile Co., Ltd., Liuzhou, China

In order to further investigate dynamic characteristics of turbine runner blades under the coupling effect of vibration and crack, in this article, a runner blade with a crack was taken as the research object. The coupling effect of vibration and crack was analyzed, a nonlinear dynamic model considering the coupling of the runner blade was developed, and the vibration and fatigue characteristics were investigated. First, based on the contact characteristics of the breathing crack surfaces in the runner blade under hydraulic excitation, a breathing crack surface contact model was established. Subsequently, a nonlinear dynamic model considering the coupling effect of vibration and crack was obtained. The crack surface contact force and crack stiffness matrix were established and the vibration and fatigue characteristics were analyzed. Finally, the feasibility of the dynamic model was verified by a case study, and the dynamic and vibration fatigue characteristics under the coupling effect of vibration and crack were revealed. The research results show that with propagation of the crack, the crack surface contact force increases and the dynamic stress amplitude at the crack tip increases as well. When the sum of the frequency of the hydraulic excitation and the crack surface contact force acting on the runner blade is close to the natural frequency of the runner blade, a combined resonance will occur. When the coupling effect of vibration and crack is taken into consideration, the vibration fatigue crack propagation model is more accurate and can provide a basis for fatigue strength and life prediction of runner blades.

Keywords: runner blade, vibration and crack coupling effect, dynamic model, nonlinear, vibration fatigue

1. Introduction

Runner blades are the main force bearing and transmitting components of hydraulic turbine generator units. Under the action of long-term hydraulic excitation, runner blades often experience complex vibration phenomena, and long-term vibration can lead to generation of fatigue cracks in different degrees and different ways. The generation of fatigue cracks can further aggravate the vibration of runner blades, causing a significant decline in the dynamic performance of the unit, and even affect its safety. In order to assess the operation efficiency and reliability of hydraulic turbines, it is necessary to develop a dynamic model of runner blade with cracks.

Currently, the available research on dynamic models of runner blades with cracks has mainly considered the effect of fluid-solid coupled as well as the effects of hydraulic parameters, structural parameters, and crack parameters and has developed dynamic models of runner blades through simulation and theoretical analysis. For instance, Yang *et al.* (2014)

used a singular element of the Ansys software to simulate the tip effect of cracks. A two-dimensional finite element analysis model of the crack was developed, and then, a dynamic model of a blade with crack was constructed. In another study, Fernandes *et al.* (2016) constructed a finite element model of a crack by using mixed-type finite elements, and developed a dynamic model of a cracked blade with different crack angles. However, under hydraulic excitation, the runner blade crack can expand changing the stiffness and resulting in a change of the dynamic response and the crack propagation rate. The dynamic response and crack propagation rate affect each other. This phenomenon is called the coupling effect between vibration and crack propagation. This coupling relationship can affect vibration characteristics and lead to crack arrest and instability propagation of the runner blade. In order to better reveal the vibration and fatigue characteristics of the runner blades, it is necessary to take the coupling relationship between vibration and fatigue cracks propagation into consideration.

At present, the research on the coupling of vibration and crack has been mainly focused on two aspects: crack stiffness and crack surface contact force. In terms of crack stiffness, scholars have considered changes in the stiffness during crack opening and closing, and have developed breathing crack models. For example, Chondros *et al.* (2001) used a nonlinear model to simulate crack stiffness and investigate vibration characteristics of a cracked beam. Liu and Chen (2010) studied the coupling problem between vibration and fatigue crack propagation of cracked beams using a single degree-of-freedom spring vibrator model and a nonlinear breathing crack stiffness model. Nevertheless, the study ignored the opening-closing phenomenon of the breathing crack, which is local contact behavior. Andreaus and Baragatti (2011) developed a contact finite element model to investigate forced vibration of structures containing cracks. The contact finite element breathing crack model considered elastic deformation when simulating the opening and closing of cracks, increasing the accuracy of the simulated stiffness changes. However, during the opening and closing process of the breathing crack, contact forces are generated on the crack surface, thus, it is necessary to study the contact forces on the crack surface in depth. For instance, Kucher *et al.* (2007) considered the contact on a blade breathing crack surface as a friction-free contact problem, introduced nonlinear contact stiffness at the crack as a penalty factor, and obtained an approximate expression of the contact force on the crack surface. To solve the convergence problem, Duan and Singh (2007) introduced a tangent smooth function into the Kucher equation, combining the Lagrange multiplier and penalty function methods in a contact problem. Bednarz (2017) considered the effect of crack parameters such as the crack gap on the crack surface contact force of a blade structure, and established an expression for the crack surface contact force using the penalty stiffness method. Although the crack stiffness and surface contact force models constructed in the above research included structural material parameters and crack parameters, the effect of vibration characteristics on the crack stiffness and surface contact force was not taken into consideration. The vibration characteristics affect the crack opening-closing cycle as well as the gap size of the crack during each cycle, which in turn affect the crack stiffness and contact force characteristics on the crack surface. Therefore, it is necessary to take into account the effect of vibration characteristics and develop a mathematical model able to reflect the internal relationship between crack stiffness and crack surface contact force characteristics.

Taking a turbine runner blade with cracks as the research object, this paper constructs a breathing crack contact model of a runner blade, develops a crack stiffness model including structural parameters, material parameters, crack parameters and vibration characteristics, formulates an analytical equation of the crack surface contact force, and obtains a nonlinear dynamic model which couples the vibration and crack propagation characteristics of the runner blade. The dynamic characteristics are obtained by decoupling the dynamic model, and then, the fatigue crack propagation model of the runner blade is obtained.

2. Breathing crack contact model

The blade can be considered as a shell structure. In order to develop an analytical model for the surface contact of breathing cracks in the blade excited by hydraulic excitation, the following assumptions need to be introduced:

- (1) It is assumed that the surface contact behavior of the breathing crack is based on a gradual opening and closing process, the change trend of which is linear.
- (2) When the crack surfaces contact with each other, the effect of axial displacement is relatively small and can be ignored, and only the effect of the radial displacement along the contact surfaces of the crack on the contact force is taken into consideration.
- (3) According to the opening closing behavior characteristics of breathing cracks, the contact between corresponding point pairs on the crack surfaces can be used to simulate this behavior.

Based on the above assumptions, a breathing crack surface contact model of a runner blade was developed, as shown in Fig. 1. According to the third assumption of the breathing crack contact model, two groups of corresponding crack contact point-pairs were: point a to point b (upper surface), and point a' to point b' (lower surface). During the actual movement of the runner blade, two forms of contact behavior on the crack surface of the runner blade can occur. The first form is displayed in Fig 1 (II) and the second in Fig. 1 (III).

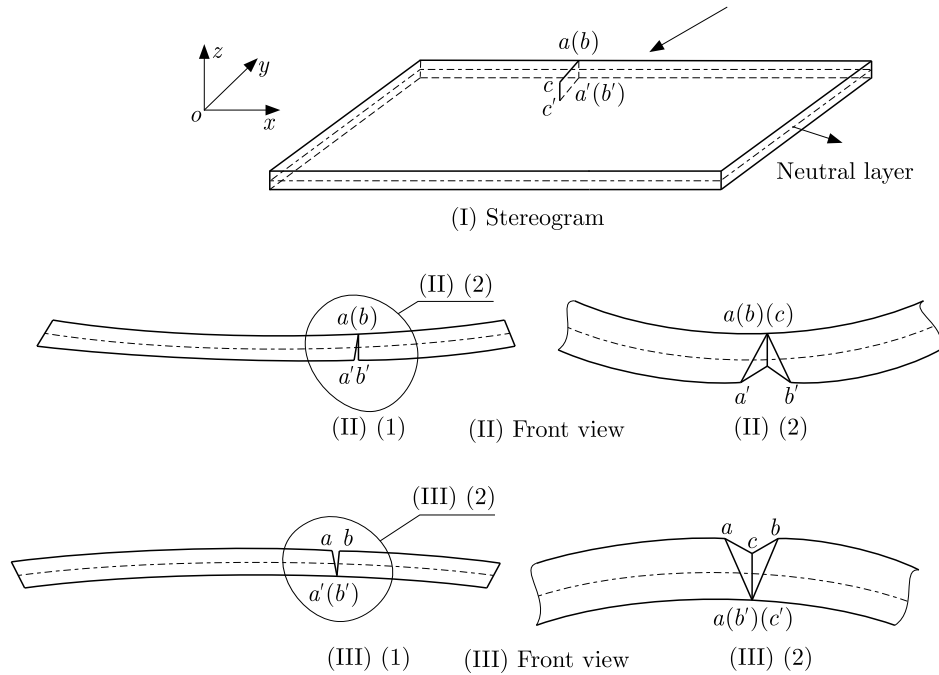


Fig. 1. The breathing crack surfaces contact model of the turbine runner blade

3. Coupling effect of vibration and crack

3.1. Crack surface contact force

Based on the shell-like mechanical model of the breathing crack surface of the blade shown in Fig. 1. When the crack opens, the surface contact force of the breathing crack in the local coordinate system can be expressed as (Luo *et al.*, 2019)

$$f'_a = -K^*(\bar{u}_a - \bar{u}_b - b_c)\delta(\bar{u}_a - \bar{u}_b - b_c) \quad f'_b = -f'_a \quad (3.1)$$

and

$$f'_{a'} = -K^*(\bar{u}_{a'} - \bar{u}_{b'} - b_c)\delta(\bar{u}_{a'} - \bar{u}_{b'} - b_c) \quad f'_b = -f'_{a'} \quad (3.2)$$

Equation (3.1) is the crack surface contact force in the first contact form, f'_a and f'_b , represent the crack surface contact force acting on points a and b , respectively. Similarly, Eqs. (3.2) is the crack surface contact force in the second contact form, $f'_{a'}$ and $f'_{b'}$ represent the crack surface contact force acting on points a' and b' , respectively. In addition, $\delta(\bar{u}_a - \bar{u}_b - b_c)$ is the unit step function, which expressed as

$$\delta(\bar{u}_a - \bar{u}_b - b_c) = \begin{cases} 1 & \text{for } \bar{u}_a - \bar{u}_b - b_c \geq 0 \\ 0 & \text{for } \bar{u}_a - \bar{u}_b - b_c < 0 \end{cases}$$

Moreover, \bar{u}_a and \bar{u}_b represent the radial displacement of points a and b , respectively, along the x -axis in the local coordinate system, $\bar{u}_{a'}$ and $\bar{u}_{b'}$ represent the radial displacement of points a' and b' , respectively, along the x -axis in the local coordinate system, b_c is the crack gap width, and K^* is the contact stiffness of the shell element, also called penalty stiffness, which can be expressed as

$$K^* = \frac{EA_c^2}{3(1-2\nu)V} \quad (3.3)$$

where V is the volume of the crack contact area of a plane shell element, A_c is the crack contact area of a plane shell element, ν is Poisson's ratio of the runner blade material, and E is its elastic modulus.

Subsequently, \bar{u}_a and \bar{u}_b in Eqs. (3.1) and $\bar{u}_{a'}$, $\bar{u}_{b'}$ in Eqs. (3.2), can be calculated based on the neutral surface of the crack, and the distance between the contact-point pair can be transformed into the displacement of the corresponding points A and A' on the neutral surface. When the first contact form is expressed in the local coordinate system of the crack in Fig. 1 (II), \bar{u}_a and \bar{u}_b in Eqs. (3.1) can be expressed as follows

$$\bar{u}_a = \bar{u}_A + \frac{h}{2}\bar{\theta}_{yA} \quad \bar{u}_b = \bar{u}_{A'} + \frac{h}{2}\bar{\theta}_{yA'} \quad (3.4)$$

where \bar{u}_A and $\bar{u}_{A'}$ represent the lateral displacement of points A and A' along the x -axis, $\bar{\theta}_{yA}$ and $\bar{\theta}_{yA'}$ represent the angular displacement of points A and A' around the y -axis, and h denotes the thickness of the shell element.

When the second contact form is expressed in the local coordinate system of the crack in Fig. 1 (III), $\bar{u}_{a'}$ and $\bar{u}_{b'}$ in Eqs. (3.2) can be expressed as follows

$$\bar{u}_{a'} = \bar{u}_A - \frac{h}{2}\bar{\theta}_{yA} \quad \bar{u}_{b'} = \bar{u}_{A'} - \frac{h}{2}\bar{\theta}_{yA'} \quad (3.5)$$

For the first contact form, the contact force acting on the crack surface of points a and b can be obtained by substituting Eq. (3.4) into Eqs. (3.1)

$$f'_a = -K^* \left[\bar{u}_A - \bar{u}_{A'} + \frac{h}{2}(\bar{\theta}_{yA} - \bar{\theta}_{yA'}) - b_c \right] \delta \left[\bar{u}_A - \bar{u}_{A'} + \frac{h}{2}(\bar{\theta}_{yA} - \bar{\theta}_{yA'}) - b_c \right] \quad (3.6)$$

$$f'_b = -f'_a$$

For the second contact form, the contact force acting on the crack surface of points a' and b' can be obtained by substituting Eqs. (3.5) into Eqs. (3.2)

$$f'_{a'} = -K^* \left[\bar{u}_A - \bar{u}_{A'} - \frac{h}{2}(\bar{\theta}_{yA} - \bar{\theta}_{yA'}) - b_c \right] \delta \left[\bar{u}_A - \bar{u}_{A'} - \frac{h}{2}(\bar{\theta}_{yA} - \bar{\theta}_{yA'}) - b_c \right] \quad (3.7)$$

$$f'_{b'} = -f'_{a'}$$

The radial and angular displacement of points A and A' in the local coordinate system of the crack in Eqs. (3.6) and (3.7) can be expressed by a displacement interpolation function. Therefore, the contact force acting on the crack surface of points a and b in the first type of contact can be expressed as

$$f'_a = -K^*(\boldsymbol{\psi}_1 \mathbf{P}\mathbf{u} - b_c)\delta(\boldsymbol{\psi}_1 \mathbf{P}\mathbf{u} - b_c) \quad f'_b = -f'_a \quad (3.8)$$

where $\boldsymbol{\psi}_1$ is 1×20 row vector, and $(\boldsymbol{\psi}_1)_1 = b_c/(2a)$, $(\boldsymbol{\psi}_1)_3 = [3h/(8a^3)](2l_c b_c + b_c^2)$, $(\boldsymbol{\psi}_1)_5 = (2ab_c h - 3b_c^2 h - 6b_c l_c h)/(8a^2)$, $(\boldsymbol{\psi}_1)_{16} = -b_c/(2a)$, $(\boldsymbol{\psi}_1)_{18} = -[3h/(8a^3)](2l_c b_c + b_c^2)$, $(\boldsymbol{\psi}_1)_{20} = -(-2ab_c h - 3b_c^2 h - 6b_c l_c h)/(8a^2)$, and the rest are zero, which is related to the structural parameters and crack parameters of the shell element. In addition, l_c is the length of the crack from the left end of the plane shell element.

Similarly, the crack surface contact force in the second type of contact can be expressed as

$$f'_{a'} = -K^*(\boldsymbol{\psi}_2 \mathbf{P}\mathbf{u} - b_c)\delta(\boldsymbol{\psi}_2 \mathbf{P}\mathbf{u} - b_c) \quad f'_{b'} = -f'_{a'} \quad (3.9)$$

where $\boldsymbol{\psi}_2$ is 1×20 row vector, and $(\boldsymbol{\psi}_2)_1 = b_c/(2a)$, $(\boldsymbol{\psi}_2)_3 = -[3h/(8a^3)](2l_c b_c + b_c^2)$, $(\boldsymbol{\psi}_2)_5 = -(2ab_c h - 3b_c^2 h - 6b_c l_c h)/(8a^2)$, $(\boldsymbol{\psi}_2)_{16} = -b_c/(2a)$, $(\boldsymbol{\psi}_2)_{18} = [3h/(8a^3)](2l_c b_c + b_c^2)$, $(\boldsymbol{\psi}_2)_{20} = (-2ab_c h - 3b_c^2 h - 6b_c l_c h)/(8a^2)$, and the other elements are zero, which is related to the structural parameters and crack parameters of the shell element.

According to Eqs. (3.8) and (3.9), the contact force on the crack surface is affected by vibration characteristics, which are related to material parameters, such as the elastic modulus and Poisson's ratio, structural parameters such as length and thickness of the shell element, crack parameters such as crack length, gap width, crack angle, contact area and contact area volume, vibration characteristics including radial displacement along x -axis and the angular displacement around the y -axis.

According to Eqs. (3.8) and (3.9), the crack surface contact force of a shell element includes two step functions, $(\boldsymbol{\psi}_1 \mathbf{P}\mathbf{u} - b_c)\delta(\boldsymbol{\psi}_1 \mathbf{P}\mathbf{u} - b_c)$ and $(\boldsymbol{\psi}_2 \mathbf{P}\mathbf{u} - b_c)\delta(\boldsymbol{\psi}_2 \mathbf{P}\mathbf{u} - b_c)$, which are nonlinear terms, thus, the crack surface contact force is a nonlinear force.

3.2. Crack stiffness matrix

According to deformation characteristics of plane shell elements with cracks under the action of crack propagation, strain energy is released. In addition, according to the stress characteristics of runner blades with cracks, considering only the strain energy released by type I (open type) and type II (sliding type) cracks, the strain energy P_c released due to crack propagation can be expressed as

$$P_c = \frac{1}{E} \int_{A_c} (K_I^2 + K_{II}^2) dA_c \quad (3.10)$$

where K_I and K_{II} correspond to mode I and II stress intensity factors at different crack inclination angles, which can be expressed as follows

$$K_I = F_I(\alpha)\sigma_\alpha\lambda_I(l)\sqrt{\pi l} \quad K_{II} = F_{II}(\alpha)\tau_\alpha\lambda_{II}(l)\sqrt{\pi l} \quad (3.11)$$

where α is the crack propagation angle, σ_α is the normal stress along the crack propagation angle direction at any time, τ_α is the shear stress along the crack propagation angle direction at any time. $F_I(\alpha)$ and $F_{II}(\alpha)$ are the propagation angle correction coefficients of mode I and II cracks, respectively, which can be determined based on the crack propagation angle α , $\lambda_I(l)$ and $\lambda_{II}(l)$ represent the stress intensity factor correction functions of mode I and II cracks, respectively, which can be determined based on relative length of the crack.

Considering large geometric deformation of the runner blade and ignoring the effect of bending deformation of the y -axis, the displacement-strain relationship for the crack section of the plane shell element can be expressed as

$$\begin{aligned}\varepsilon_{l_x} &= \frac{\partial u}{\partial x} + z \frac{\partial^2 w}{\partial x^2} + \frac{1}{2} \left(\frac{\partial w}{\partial x} \right)^2 & \varepsilon_y &= 0 \\ \gamma_{x_y} &= \frac{\partial u}{\partial y} + \frac{\partial v}{\partial x} + 2z \frac{\partial^2 w}{\partial x \partial y} + \frac{\partial w}{\partial x} \frac{\partial w}{\partial y}\end{aligned}\quad (3.12)$$

Equation (3.12) can be transformed into a matrix form as follows

$$\boldsymbol{\varepsilon}_c = \tilde{\mathbf{S}}_0 \mathbf{u} + \frac{1}{2} \sum_{j=1}^3 \mathbf{k}_j \mathbf{u}^T \tilde{\mathbf{S}}_j \mathbf{u} \quad (3.13)$$

where

$$\boldsymbol{\varepsilon}_c = \begin{bmatrix} \varepsilon_{l_x} \\ 0 \\ \gamma_{l_{xy}} \end{bmatrix} \quad \tilde{\mathbf{S}}_0 = \begin{bmatrix} \frac{\partial}{\partial x} & 0 & z \frac{\partial^2}{\partial x^2} \\ 0 & 0 & 0 \\ \frac{\partial}{\partial y} & \frac{\partial}{\partial x} & 2z \frac{\partial^2}{\partial x \partial y} \end{bmatrix} \mathbf{N}$$

$$\mathbf{N} = \begin{bmatrix} N_{u1} & 0 & 0 & 0 & 0 & N_{u2} & 0 & 0 & 0 & 0 & N_{u3} & 0 & 0 & 0 & 0 & N_{u4} & 0 & 0 & 0 & 0 \\ 0 & N_{v1} & 0 & 0 & 0 & 0 & N_{v2} & 0 & 0 & 0 & 0 & N_{v3} & 0 & 0 & 0 & 0 & N_{v4} & 0 & 0 & 0 \\ 0 & 0 & N_{w1} & N_{\theta_{x1}} & N_{\theta_{y1}} & 0 & 0 & N_{w2} & N_{\theta_{x2}} & N_{\theta_{y2}} & 0 & 0 & N_{w3} & N_{\theta_{x3}} & N_{\theta_{y3}} & 0 & 0 & N_{w4} & N_{\theta_{x4}} & N_{\theta_{y4}} \end{bmatrix}$$

and N_{ui} , N_{vi} , N_{wi} , $N_{\theta_{xi}}$, $N_{\theta_{yi}}$ ($i = 1, 2, 3, 4$) are form functions, \mathbf{k}_j ($j = 1, 2, 3$), where $\mathbf{k}_1 = [1, 0, 0]^T$, $\mathbf{k}_2 = [0, 1, 0]^T$, $\mathbf{k}_3 = [0, 0, 1]^T$, $\tilde{\mathbf{S}}_j$ ($j = 1, 2, 3$) is 20×20 matrix, where

$$\begin{aligned}\tilde{\mathbf{S}}_1 &= \begin{bmatrix} \frac{\partial \mathbf{N}_3^T}{\partial x} & \mathbf{O}_{20 \times 1} & \mathbf{O}_{20 \times 1} \end{bmatrix} \begin{bmatrix} \frac{\partial \mathbf{N}_3}{\partial x} \\ \mathbf{O}_{1 \times 20} \\ \mathbf{O}_{1 \times 20} \end{bmatrix} & \tilde{\mathbf{S}}_2 &= \begin{bmatrix} \mathbf{O}_{20 \times 1} & \mathbf{O}_{20 \times 1} & \mathbf{O}_{20 \times 1} \end{bmatrix} \begin{bmatrix} \frac{\partial \mathbf{N}_3}{\partial x} \\ \mathbf{O}_{1 \times 20} \\ \mathbf{O}_{1 \times 20} \end{bmatrix} \\ \tilde{\mathbf{S}}_3 &= \begin{bmatrix} \frac{\partial \mathbf{N}_3^T}{\partial y} & \frac{\partial \mathbf{N}_3^T}{\partial x} & \mathbf{O}_{20 \times 1} \end{bmatrix} \begin{bmatrix} \frac{\partial \mathbf{N}_3}{\partial x} \\ \mathbf{O}_{1 \times 20} \\ \mathbf{O}_{1 \times 20} \end{bmatrix}\end{aligned}$$

and

$$\mathbf{N}_3 = [0, 0, N_{w1}, N_{\theta_{x1}}, N_{\theta_{y1}}, 0, 0, N_{w2}, N_{\theta_{x2}}, N_{\theta_{y2}}, 0, 0, N_{w3}, N_{\theta_{x3}}, N_{\theta_{y3}}, 0, 0, N_{w4}, N_{\theta_{x4}}, N_{\theta_{y4}}]$$

The relationship between stress and strain is

$$\boldsymbol{\sigma}_c = \mathbf{D} \boldsymbol{\varepsilon}_c \quad (3.14)$$

where $\boldsymbol{\sigma}_c = [\sigma_{l_x}, 0, \tau_{l_{xy}}]^T$, \mathbf{D} is the elastic matrix of the shell element, which can be expressed as

$$\mathbf{D} = \frac{E}{1 - \nu^2} \begin{bmatrix} 1 & \nu & 0 \\ \nu & 1 & 0 \\ 0 & 0 & \frac{1-\nu}{2} \end{bmatrix} \quad (3.15)$$

By substituting Equations (3.11)₁ to (3.14) into Eq. (3.10), the following expression can be obtained

$$\begin{aligned}P_c &= \frac{1}{2} \mathbf{u}^T \mathbf{k}_c \mathbf{u} + \frac{\pi l}{4E} \int_{A_c} \sum_{j=1}^3 \sum_{k=1}^3 \mathbf{u}^T \mathbf{k}_j^T \mathbf{u} \tilde{\mathbf{h}}_{jk} \mathbf{u}^T \mathbf{k}_k \mathbf{u} dA_c \\ &+ \frac{\pi l}{2E} \int_{A_c} \sum_{j=1}^3 (\mathbf{u}^T \tilde{\mathbf{g}}_j \mathbf{u}^T \mathbf{k}_j \mathbf{u} + \mathbf{u}^T \mathbf{k}_j^T \mathbf{u} \tilde{\mathbf{g}}_j^T \mathbf{u}) dA_c\end{aligned}\quad (3.16)$$

where

$$\tilde{\mathbf{g}}_j = \tilde{\mathbf{S}}_0^T \mathbf{D}^T \boldsymbol{\lambda} \tilde{\mathbf{S}}_j \quad \tilde{\mathbf{h}}_{jk} = \tilde{\mathbf{S}}_j^T \mathbf{D}^T \boldsymbol{\lambda} \mathbf{D} \tilde{\mathbf{S}}_k \quad \boldsymbol{\lambda} = \begin{bmatrix} F_I^2(\alpha) \lambda_I^2 & 0 & 0 \\ 0 & 0 & 0 \\ 0 & 0 & F_{II}^2(\alpha) \lambda_{II}^2 \end{bmatrix}$$

Subsequently, the shell element stiffness matrix \mathbf{k}_c caused by crack propagation can be obtained

$$\mathbf{k}_c = \frac{2\pi l}{E} \int_{A_c} \tilde{\mathbf{S}}_0^T \mathbf{D}^T \boldsymbol{\lambda} \mathbf{D} \tilde{\mathbf{S}}_0 dA_c \quad (3.17)$$

According to Eq. (3.17), the crack-stiffness-matrix is affected by the vibration characteristics, which are related to material parameters, such as the elastic modulus and Poisson's ratio, structural parameters such as length and thickness of the shell element, crack parameters such as crack length, crack propagation angle, crack contact area and contact area volume, and vibration characteristics such as normal and shear stress amplitudes.

4. Dynamic coupling model of vibration and crack

The relationship between the generalized coordinate vector \mathbf{i} of element \mathbf{u}_i and the generalized coordinate vector \mathbf{U} of the shell structure in the global coordinate system can be expressed as

$$\mathbf{u}_i = \mathbf{R}_i \mathbf{B}_i \mathbf{U} \quad (4.1)$$

where \mathbf{B}_i is the coordinate matrix between the unit number and system number, and \mathbf{R}_i is the conversion matrix between the coordinates unit \mathbf{i} and the global coordinates.

For large geometric deformation and the crack surface contact force, the dynamic equation of a runner blade with a crack can be written as follows

$$\begin{aligned} & (\mathbf{M}_t + \mathbf{M}_p) \ddot{\mathbf{U}} + \mathbf{C} \dot{\mathbf{U}} + (\mathbf{K} - \mathbf{K}_c) \mathbf{U} = \mathbf{F} + \mathbf{F}' - \mathbf{M}_d \ddot{\mathbf{U}}_d \\ & + \frac{3}{2} \sum_{i=1}^n \sum_{j=1}^3 \int_V (\mathbf{G}_{ji} \mathbf{U}^T \mathbf{k}_j \mathbf{U} + 2 \mathbf{U}^T \mathbf{G}_{ji} \mathbf{k}_j \mathbf{U}) dV \\ & - \sum_{i=1}^n \int_{A_{ci}} \frac{3\pi l_i}{2E} \sum_{j=1}^3 (\tilde{\mathbf{G}}_{ji} \mathbf{U}^T \mathbf{k}_j \mathbf{U} + 2 \mathbf{U}^T \tilde{\mathbf{G}}_{ji} \mathbf{k}_j \mathbf{U}) dA_{ci} \\ & - \sum_{i=1}^n \frac{\pi l_i}{E} \int_{A_{ci}} \sum_{j=1}^3 \sum_{k=1}^3 \mathbf{k}_j^T \mathbf{U} \tilde{\mathbf{H}}_{jki} \mathbf{U}^T \mathbf{k}_k \mathbf{U} dA_{ci} + \frac{1}{2} \sum_{i=1}^n \sum_{j=1}^3 \sum_{k=1}^3 \int_V \mathbf{k}_j^T \mathbf{U} \mathbf{H}_{jki} \mathbf{U}^T \mathbf{k}_k \mathbf{U} dV \end{aligned} \quad (4.2)$$

where $\mathbf{G}_{ji} = \mathbf{B}_i^T \mathbf{R}_i^T \mathbf{g}_{ji}$, $\tilde{\mathbf{G}}_{ji} = \mathbf{B}_i^T \mathbf{R}_i^T \tilde{\mathbf{g}}_{ji}$, $\mathbf{H}_{jki} = \mathbf{B}_i^T \mathbf{R}_i^T \mathbf{h}_{jki} \mathbf{R}_i \mathbf{B}_i$, $\tilde{\mathbf{H}}_{jki} = \mathbf{B}_i^T \mathbf{R}_i^T \tilde{\mathbf{h}}_{jki} \mathbf{R}_i \mathbf{B}_i$. In addition, \mathbf{U} , $\dot{\mathbf{U}}$ and $\ddot{\mathbf{U}}$ correspond to the generalized coordinate vector, velocity vector, and acceleration vector in the global coordinate system of the blade with crack, $\ddot{\mathbf{U}}_d$ is the rigid body acceleration vector, $\mathbf{M}_d \ddot{\mathbf{U}}_d$ is the self-excited inertial force of the system, \mathbf{M}_t and \mathbf{M}_p are the mass matrix and additional mass matrix, respectively, \mathbf{C} is the damping matrix, \mathbf{K} is the stiffness matrix, \mathbf{F} and \mathbf{F}' are the hydraulic excitation and crack surface contact force, respectively.

According to Eq. (4.2), the dynamic equation of the blade with the crack includes the nonlinear crack surface contact force, a nonlinear term representing the large geometric deformation of the blade $\sum_{i=1}^n \sum_{j=1}^3 \int_V (\mathbf{G}_{ji} \mathbf{U}^T \mathbf{k}_j \mathbf{U} + 2 \mathbf{U}^T \mathbf{G}_{ji} \mathbf{k}_j \mathbf{U}) dV$, and a nonlinear term representing the crack strain energy of the blade $-\sum_{i=1}^n \int_{A_{ci}} [\pi l_i / (2E)] \sum_{j=1}^3 (\tilde{\mathbf{G}}_{ji} \mathbf{U}^T \mathbf{k}_j \mathbf{U} + 2 \mathbf{U}^T \tilde{\mathbf{G}}_{ji} \mathbf{k}_j \mathbf{U}) dA_{ci}$,

therefore the dynamic equation of the blade with the crack is a nonlinear equation. In the dynamic equation of the blade, the \mathbf{F}' (nonlinear crack surface contact force) and $\mathbf{K}_c \mathbf{U}$ (elastic restoring force) terms caused by the crack as well as the nonlinear terms generated by crack strain energy of the blade include not only crack parameters, but also vibration parameters. Consequently, this is a coupling relationship between vibration and the crack.

5. Vibration and fatigue characteristics of runner blades

5.1. Dynamic characteristics of runner blades

By solving Eq. (4.2) using the multi-scale method, the dynamic response of the blade with the crack can be obtained

$$\mathbf{U} = \boldsymbol{\varphi} \boldsymbol{\eta} \quad \dot{\mathbf{U}} = \boldsymbol{\varphi} \dot{\boldsymbol{\eta}} \quad \ddot{\mathbf{U}} = \boldsymbol{\varphi} \ddot{\boldsymbol{\eta}} \quad (5.1)$$

where $\boldsymbol{\varphi}$ is the regular modal matrix and $\boldsymbol{\eta}$ is the corresponding modal coordinate array of the blade. Subsequently, the approximate solution of the displacement response \mathbf{U} of the blade with the crack can be expressed as

$$\mathbf{U} = \sum_{r=1}^n \boldsymbol{\eta}_r \boldsymbol{\varphi}^{(r)} \quad (5.2)$$

Based on the developed finite element model of the blade, the relationship between displacement and strain is as follows

$$\boldsymbol{\varepsilon} = \mathbf{S}_0 \mathbf{u} + \frac{1}{2} \sum_{j=1}^3 \mathbf{S}_j \mathbf{u}^T \mathbf{k}_j \mathbf{u} \quad (5.3)$$

where $\boldsymbol{\varepsilon} = [\varepsilon_x, \varepsilon_y, \gamma_{xy}]^T$, can be expressed as

$$\begin{aligned} \varepsilon_x(x, t) &= \frac{\partial u}{\partial x} + z \frac{\partial^2 w}{\partial x^2} + \frac{1}{2} \left(\frac{\partial w}{\partial x} \right)^2 & \varepsilon_y(x, t) &= \frac{\partial v}{\partial y} + z \frac{\partial^2 w}{\partial y^2} + \frac{1}{2} \left(\frac{\partial w}{\partial y} \right)^2 \\ \gamma_{xy}(x, t) &= \frac{\partial u}{\partial y} + \frac{\partial v}{\partial x} + 2z \frac{\partial^2 w}{\partial x \partial y} + \frac{\partial w}{\partial x} \frac{\partial w}{\partial y} \end{aligned} \quad (5.4)$$

where \mathbf{S}_j ($j = 1, 2, 3$) is 20×20 matrix, and

$$\begin{aligned} \mathbf{S}_1 &= \begin{bmatrix} \frac{\partial \mathbf{N}_3^T}{\partial x} & \mathbf{O}_{20 \times 1} & \mathbf{O}_{20 \times 1} \end{bmatrix} \begin{bmatrix} \frac{\partial \mathbf{N}_3}{\partial x} \\ \frac{\partial \mathbf{N}_3}{\partial y} \\ \mathbf{O}_{1 \times 20} \end{bmatrix} & \mathbf{S}_2 &= \begin{bmatrix} \mathbf{O}_{20 \times 1} & \frac{\partial \mathbf{N}_3^T}{\partial y} & \mathbf{O}_{20 \times 1} \end{bmatrix} \begin{bmatrix} \frac{\partial \mathbf{N}_3}{\partial x} \\ \frac{\partial \mathbf{N}_3}{\partial y} \\ \mathbf{O}_{1 \times 20} \end{bmatrix} \\ \mathbf{S}_3 &= \begin{bmatrix} \frac{\partial \mathbf{N}_3^T}{\partial y} & \frac{\partial \mathbf{N}_3^T}{\partial x} & \mathbf{O}_{20 \times 1} \end{bmatrix} \begin{bmatrix} \frac{\partial \mathbf{N}_3}{\partial x} \\ \frac{\partial \mathbf{N}_3}{\partial y} \\ \mathbf{O}_{1 \times 20} \end{bmatrix} \end{aligned}$$

The relationship between stress and strain is

$$\boldsymbol{\sigma} = \mathbf{D} \boldsymbol{\varepsilon} \quad (5.5)$$

Refer to Eq. (3.15) for the \mathbf{D} matrix above. By combining Eqs. (4.1), (5.3) and (5.5), the dynamic stress at any position of the blade with the crack can be obtained as follows

$$\boldsymbol{\sigma} = \mathbf{D} \mathbf{S}_0 \mathbf{R}_i \mathbf{B}_i \mathbf{U} + \frac{1}{2} \sum_{j=1}^3 \mathbf{D} \mathbf{k}_j \mathbf{U}^T \mathbf{B}_i^T \mathbf{R}_i^T \mathbf{S}_j \mathbf{R}_i \mathbf{B}_i \mathbf{U} \quad (5.6)$$

5.2. Vibration fatigue characteristics of blades with cracks

According to the Paris fatigue crack propagation model, the fatigue crack propagation rate of a runner blade with a crack can be expressed as

$$\frac{dl}{dN} = C_0(\Delta K)^m \quad (5.7)$$

where l is the crack length of the member with the crack, N is the number of cycles of dynamic stress, m and C_0 are material constants of the members with the crack, and ΔK is the stress intensity factor amplitude. Considering the contact and vibration characteristics of the crack surface, the amplitude of the stress intensity factor can be expressed as

$$\Delta K = \frac{1}{2} \cos \frac{\alpha}{2} [\Delta K_{\text{I}}(1 + \cos \alpha) - 3\Delta K_{\text{II}} \sin \alpha] + F(l) \frac{\Delta f(\mathbf{U})}{\sqrt{\pi l}} \quad (5.8)$$

where $F(l)$ is the crack shape correction factor, which is related to the crack size and which can be obtained from the stress intensity factor manual, ΔK_{I} and ΔK_{II} are the amplitudes of K_{I} and K_{II} , respectively, and $\Delta f(\mathbf{U})$ is the amplitude of the contact force acting on the crack surface, which can be determined by combining Equations (3.8), (3.9) and (5.2).

By substituting Eq. (5.8) into Eq. (5.7), the crack propagation rate model of the runner blade with the crack can be expressed as

$$\frac{dl}{dN} = C_0 \left(\frac{1}{2} \cos \frac{\alpha}{2} [\Delta K_{\text{I}}(1 + \cos \alpha) - 3\Delta K_{\text{II}} \sin \alpha] + F(l) \frac{\Delta f(\mathbf{U})}{\sqrt{\pi l}} \right)^m \quad (5.9)$$

According to Equations (5.6) and (5.9), due to the coupling effect between vibration and the crack, the contact force on the crack surface and the crack stiffness change continuously with propagation of the crack, resulting in a continuous change of the dynamic stress characteristics. Consequently, the crack propagation model of the runner blade is related not only to the amplitude of dynamic stress, but also to the amplitude of the contact force on the crack surface.

6. Case study

In this Section, a large Francis turbine in Guangxi is taken as an example. The main parameters of the runner are as follows: rated speed of 75 RPM, rated head of 59.4 m, rated flow of $Q_0 = 580 \text{ m}^3/\text{s}$, rated working condition of 302.5 MW, maximum runner diameter of 8.33 m, height of 5.19 m, upper crown and lower ring mass of $101.4 \cdot 10^3 \text{ kg}$ and $68 \cdot 10^3 \text{ kg}$, respectively, and upper crown and lower ring moment of inertia of $8.52 \cdot 10^5 \text{ kg}\cdot\text{m}^2$ and $1.15 \cdot 10^6 \text{ kg}\cdot\text{m}^2$, respectively. In total, 13 blades are evenly distributed in the runner. A single blade has mass of $7.7 \cdot 10^3 \text{ kg}$, width of 1.65 m, thickness of 0.62 m, elastic modulus of $E = 210 \text{ GPa}$, material density of $7.85 \cdot 10^3 \text{ kg}/\text{m}^3$, and Poisson's ratio of $\nu = 0.3$.

In actual operation, due to the thin water outlet edge of the blade and the stress concentration phenomenon at the "T-shaped" connection between the blade and upper crown, penetrating cracks often appear at the water outlet edge of the blade. Table 1 lists the statistical values of through cracks found on the outlet edge of the blade of a hydropower station. The runner blade material is ZG0Cr13Ni5Mo, the material constant is $m = 3.65$, $C_0 = 3.46 \cdot 10^{-10}$ and its allowable stress is $\sigma = 43.27 \cdot 10^7 \text{ Pa}$.

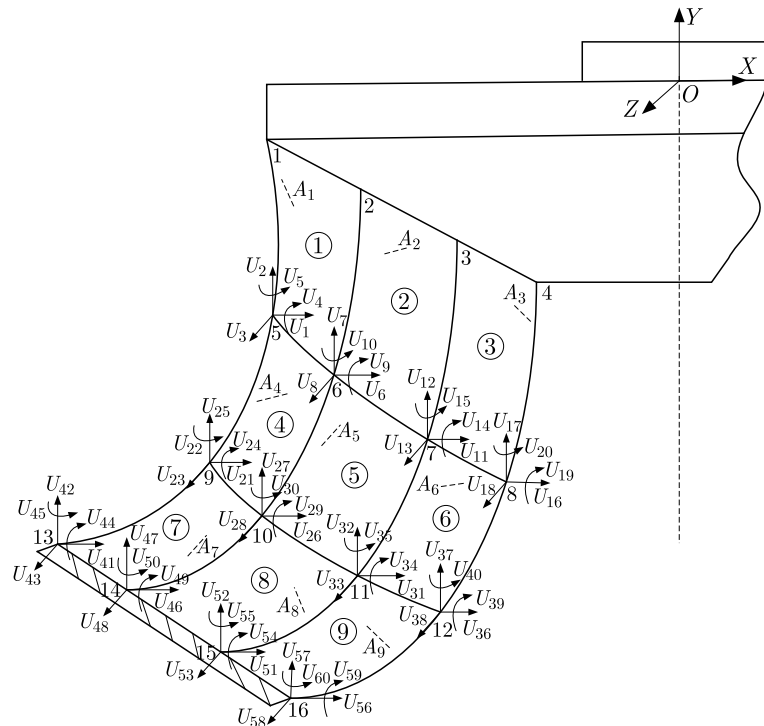
In order to verify the correctness of the developed model, No. 3 blade under rated working conditions was taken as the research object. Based on the characteristics of hydraulic excitation acting on the blade, a crack 100 mm away from the upper crown was analyzed. It was assumed that the blade contained only a single crack. Two different crack lengths of 100 mm and 150 mm

Table 1. Statistical table of through cracks on the water outlet edge of blades of a hydropower station

Blade number	Crack location	Crack type	Crack size
3	100 mm from upper crown	Through crack	150 mm
8	20 mm from lower ring	Through crack	90 mm
9	30 mm from upper crown	Through crack	140 mm
11	50 mm from lower ring	Through crack	130 mm

Table 2. Each node direction displacement representation symbols of the crack blade

Displacement in each node direction	Representation symbol
Lateral displacement along X -axis	$U_1, U_6, U_{11}, U_{16}, U_{21}, U_{26}, U_{31}, U_{36}, U_{41}, U_{46}, U_{51}, U_{56}$
Lateral displacement along Y -axis	$U_2, U_7, U_{12}, U_{17}, U_{22}, U_{27}, U_{32}, U_{37}, U_{42}, U_{47}, U_{52}, U_{57}$
Lateral displacement along Z -axis	$U_3, U_8, U_{13}, U_{18}, U_{23}, U_{28}, U_{33}, U_{38}, U_{43}, U_{48}, U_{53}, U_{58}$
Angular displacement around Z -axis	$U_4, U_9, U_{14}, U_{19}, U_{24}, U_{29}, U_{34}, U_{39}, U_{44}, U_{49}, U_{54}, U_{59}$
Angular displacement around Y -axis	$U_5, U_{10}, U_{15}, U_{20}, U_{25}, U_{30}, U_{35}, U_{40}, U_{45}, U_{50}, U_{55}, U_{60}$

**Fig. 2.** Finite element model of the runner blade with cracks

and crack gap widths of 1.6 mm and 2 mm were investigated. In order to simplify the simulation model, the runner blade was divided into 9 rectangular elements, each blade had 60 degrees-of-freedom, the element number was represented by ①, ②, A_1, A_2, \dots , indicated the crack number, the node numbers were represented by 1, 2, \dots (Table 2). The finite element model of the blade with the crack is illustrated in Fig. 2.

Time-domain simulation diagrams of the contact force on the crack surface and dynamic stress at the crack tip were obtained according to Eqs. (3.8), (3.9) and (5.6), for a crack length of 100 mm and crack gap width of 1.6 mm. The results are shown in Figs. 3a and 3b, respectively. For a crack length of 150 mm and crack gap width of 2 mm, the results are shown in Figs. 4a and 4b, respectively.

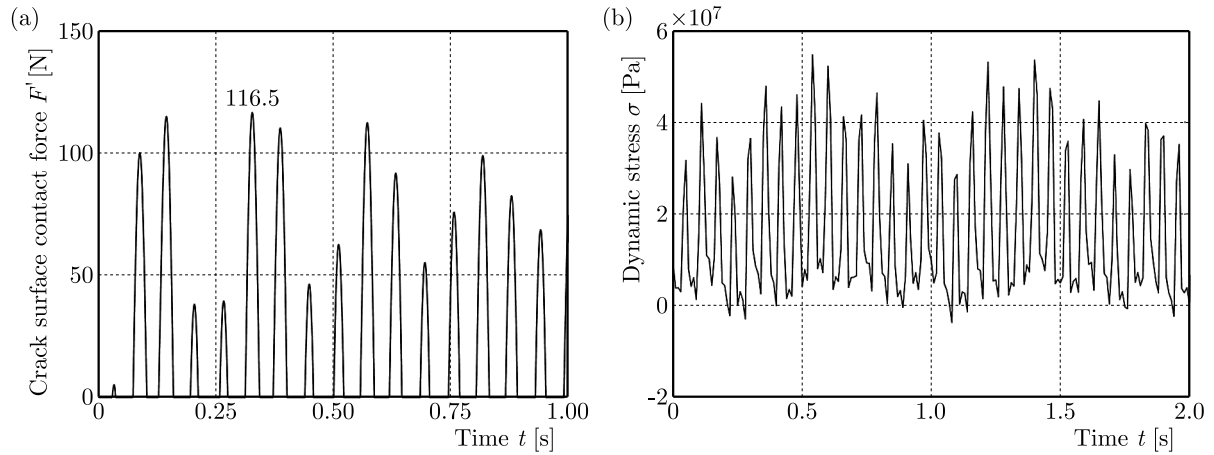


Fig. 3. (a) Simulation curve of the crack surfaces contact force and (b) time domain simulation curve crack-tip dynamic stress when the crack length was 100 mm and the crack gap width was 1.6 mm

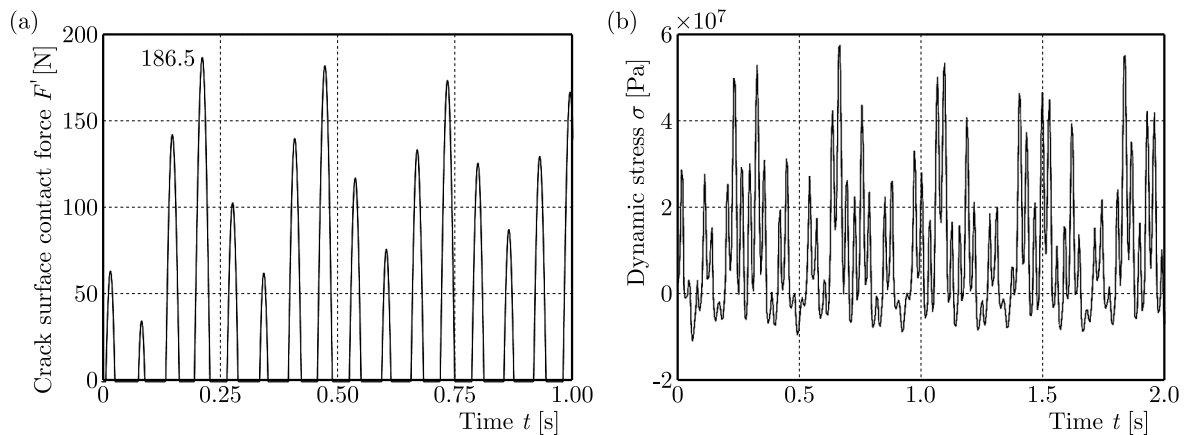


Fig. 4. (a) Simulation curve of the crack surfaces contact force and (b) time domain simulation curve crack-tip dynamic stress when the crack length was 150 mm and the crack gap width was 2 mm

According to Figs. 3a and 4a, the contact force on the crack surface increases with propagation of the crack. In addition, as the crack gap width increases, the period of the contact force on the crack surface increases as well. According to Figs. 3b and 4b, the dynamic stress amplitude at the crack tip increases with propagation of the crack.

As shown in Figs. 5a and 5b, the correctness of the developed model is verified. The fracture module in Ansys workbench was used to establish the crack, the surface unit surface body was inserted at the crack location and the grid was divided, dynamic load was applied and transient dynamic analysis was carried out. The results show that the closer the crack position is, the greater is the dynamic stress. Among them, the dynamic stress at the crack is 32.7 MPa and the mean dynamic stress in Fig. 3b is 30.1 MPa, the error is 2.6 MPa, and the error rate is 7.9%.

According to Eq. (3.17), the crack stiffness increases due to propagation of the crack, which leads to a continuous reduction of the natural frequency of the runner blade with the crack. Moreover, width of the crack gap increases due to propagation of the crack, and the period

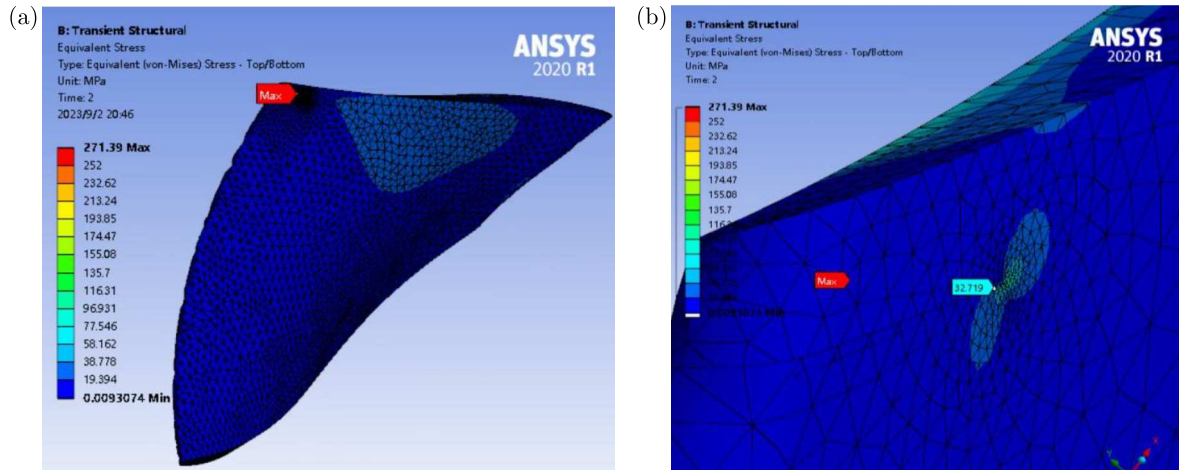


Fig. 5. (a) Blade crack model, (b) crack position force diagram

of the contact force on the crack surface increases as well. When the sum of the frequency of hydraulic excitation and the crack surface contact force acting on the blade is close to the natural frequency of the blade, a combined resonance of the runner blade will be caused. Based on the characteristics of hydraulic excitation acting on the blade, when the crack extends to 132 mm, the combined resonance will occur. By comparing Figs. 3b and 4b, it can be observed that when the crack length is 150 mm, the dynamic stress at the crack tip was more irregular than that when the crack length was 100 mm, which also provides a theoretical basis for unstable propagation of the crack under resonance.

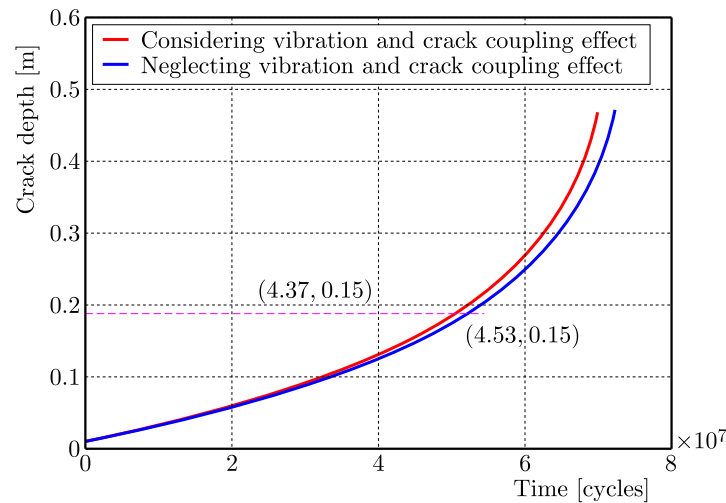


Fig. 6. Simulation curve of fatigue crack propagation

In Fig. 6, when only dynamic stress is considered without considering the coupling effect of vibration and crack, the crack propagation life curve is the blue line; and when the contact force and dynamic stress on the crack surface are considered, taking the coupling effect of vibration and crack into consideration, the crack propagation life curve is the one red. It can be observed that when the working condition was only the rated load, the crack expanded to the length of 150 mm after $4.53 \cdot 10^7$ s (524.3 days). When the coupling effect of vibration and crack was taken into consideration, the crack propagation to 150 mm took $4.42 \cdot 10^7$ s (511.6 days). According to (Yang *et al.*, 2014)], the turbine blades are mainly operated near the rated working conditions and are stopped for inspection every $4.25 \cdot 10^7$ s (491.7 days). When considering the coupling

effect of vibration and crack, the error between the simulation and test results is 4.04%, while, without considering the coupling effect of vibration and crack, the error is 6.63%. This indicates that the vibration fatigue crack propagation model considering the coupling effect of vibration and crack is more accurate, and provides a basis for fatigue strength and life prediction of blades.

7. Conclusions

- With propagation of the crack, the contact force on the crack surface increases, its period increases, and the dynamic stress amplitude at the crack tip increases as well.
- The propagation of the crack increases the crack stiffness, which leads to a continuous reduction in the natural frequency of the blade. When the sum of the frequency of hydraulic excitation and the crack surface contact force acting on the blade is close to the natural frequency of the blade, and a combined resonance occurs, which also provides a theoretical basis for unstable propagation of cracks under the resonance.
- When the coupling effect of vibration and crack is taken into consideration, the developed vibration fatigue crack propagation model is more accurate, and can provide a basis for prediction of the fatigue strength and life of the blades.

Acknowledgments

The research was supported by a doctoral start-up fund of Guangxi University of Science and Technology (No. 03210126) as well as National Natural Science Foundation of China under grants No. 22262005. The supports are gratefully acknowledged.

References

1. ANDREAUS U., BARAGATTI P., 2011, Cracked beam identification by numerically analysing the nonlinear behaviour of the harmonically forced response, *Journal of Sound and Vibration*, **330**, 4, 721-742
2. ARVIN H., BAKHTIARI-NEJAD F., 2011, Non-linear modal analysis of a rotating beam, *International Journal of Non-Linear Mechanics*, **46**, 6, 877-897
3. BEDNARZ J., 2017, Operational modal analysis for crack detection in rotating blades, *Archives of Acoustics*, **42**, 1, 105-112
4. CHONDROS T.G., DIMAROGONAS A.D., YAO J., 2001, Vibration of a beam with a breathing crack, *Journal of Sound and Vibration*, **239**, 1, 57-67
5. CUI W., WANG J., 2014, Coupling analysis of vibration and crack propagation for a cracked beam at resonant state (in Chinese), *Journal of Propulsion Technology*, **10**, 1404-1411
6. DUAN C., SINGH R., 2007, Dynamic analysis of preload nonlinearity in a mechanical oscillator, *Journal of Sound and Vibration*, **301**, 3, 963-978
7. FERNANDES R., EL-BORGI S., AHMED K., *et al.*, 2016, Static fracture and modal analysis simulation of a gas turbine compressor blade and bladed disk system, *Advanced Modeling and Simulation in Engineering Sciences*, **3**, 1, 1-23
8. Guangxi Electric Power Experimental Research Institute, Guangxi University, Datang Yantan Hydropower Plant. Dynamic stress test and crack cause analysis report of runner blade of No. 3 unit in Yantan power plant, Nanning: Guangxi Electric Power Experimental Research Institute, 1998
9. HE Q., PENG H., ZHAI P., ZHEN Y., 2016, The effects of unbalance orientation angle on the stability of the lateral torsion coupling vibration of an accelerated rotor with a transverse breathing crack, *Mechanical Systems and Signal Processing*, **75**, 330-344

10. KANG J.W., ZHANG J.F., LIU B.C., HUANG T., 2008, Improved thermal stress analysis for castings, *International Journal of Cast Metals Research*, **21**, 1-4, 324-329
11. KHORRAMI H., RAKHEJA S., SEDAGHATI R., 2017, Vibration behavior of a two-crack shaft in a rotor disc-bearing system, *Mechanism and Machine Theory*, **113**, 67-84
12. KUCHER O., KHARYTON V., LAINE J.P., *et al.*, 2007, Harmonic balance method implementation for crack breathing process simulation, *Aerospace Technique and Technology*, **44**, 8, 150-156
13. LI Z.J., WANG Y.J., LI T.H., MA X., JI J., 2019, Effect of crack surface contact forces on vibration fatigue characteristics of beam structure, *Journal of the Brazilian Society of Mechanical Sciences and Engineering*, **41**, 12, 560
14. LI Z.J., WANG Y.J., LIU F.X., *et al.*, 2020, The hydrodynamic pressure characters acting on a turbine runner blade under the vortex rope in draft tube (in Chinese), *Journal of Guangxi University (Natural Science Edition)*, **45**, 6, 1351-1358
15. LIU W.G., BARKEY M.E., 2018, The effects of breathing behaviour on crack growth of a vibrating beam, *Shock and Vibration*, **3**, 2579419.1-12
16. LIU W.G., CHEN G.P., 2010, Coupling analysis of vibration fatigue crack propagation for breathing cracked beam (in Chinese), *China Mechanical Engineering*, **21**, 23, 2798-2802
17. LUO Y., PRESAS A., WANG Z., XIAO Y., WANG H., JIANG X., 2019, Operating conditions leading to crack propagation in turbine blades of tidal barrages. Influence of head and operating mode, *Engineering Failure Analysis*, 104254
18. PARIS P., ERDOGAN F., 1963, A critical analysis of crack propagation laws, *Journal of Basic Engineering*, **85**, 4, 528-534
19. SAITO A., CASTANIER M.P., PIERRE C., POUDOU O., 2009, Efficient nonlinear vibration analysis of the forced response of rotating cracked blades, *Journal of Computational and Nonlinear Dynamics*, **4**, 1, 53-63
20. WANG Y.J., LI Z.J., LI T.H., LIU F., FU A., 2021, A mathematical model of the hydrodynamic pressure acting on a turbine runner blade under the rotor-stator interaction based on the quasi-three dimensional finite element method, *Mathematical Problems in Engineering*, **2021**, 3, 1-11
21. YANG L.F., XU H., SHE Z.P., *et al.*, 2014, Stress intensity factor for mixed mode cracks by Williams element (in Chinese), *Journal of Ship Mechanics*, **18**, 1, 115-124
22. YANG X.F., SWAMIDAS A.S.J., SESHADRI R., 2001, Crack identification in vibrating beams using the energy method, *Journal of Sound and Vibration*, **244**, 2, 339-357
23. ZHAO J.S., 2003, *Fracture Mechanics and Fracture Physics* (in Chinese), Wuhan, Huazhong University of Science and Technology Press
24. ZHU D., TAO R., XIAO R.F.A., PAN L., 2020, Solving the runner blade crack problem for a Francis hydro-turbine operating under condition-complexity, *Renewable Energy*, **149**, 298-320